EFFECTS OF SAMPLE DISTURBANCE ON LIQUEFACTION RESISTANCE AND SMALL STRAIN CHARACTERISTICS OF SANDY SOILS

Takashi KIYOTA[1] and Junichi KOSEKI[2]

ABSTRACT: To investigate the liquefaction behaviour of in-situ frozen and reconstituted samples, undrained cyclic triaxial tests were performed on two kinds of sandy soils. In order to evaluate the possible effects of sample disturbance caused by different confining pressures during thaw process of in-situ frozen samples, dynamic and static small strain characteristics were measured during isotropic consolidation and liquefaction stages, which would reflect the soil structure. Decrease in the small strain stiffness was observed in case of the frozen specimen that was thawed at low confining pressure, and it may be linked with the change in the liquefaction resistance of the specimen.

Key Words: Liquefaction, Laboratory test, Small strain, Aging, Sandy soil, Sample disturbance

INTRODUCTION

Laboratory test on in-situ frozen sandy samples is a well-known high quality method for understanding the actual soil behaviour under working loads as well as small to moderate earthquake loads. However, in-situ frozen sample may be disturbed due to possible expansion during ground freezing, and the disturbance would affect significantly the test results. Yoshimi et al. (1978) and Goto (1993) showed the limiting values of the amount of fines and the level of confining stress for preventing disturbance due to a freeze-thaw cycle.

The small strain quasi-elastic stiffness is one of the important parameters that reflect the soil structure as well as the extent of specimen disturbance. Because the small stress-strain behaviour reflects the current fabric, while the large stress-strain behaviour is affected by fabric changes. Several laboratory tests have been performed with static or dynamic small strain measurements to evaluate quasi-elastic stiffness during liquefaction (Tanizawa et al., 1994; Koseki et al., 2000). In addition, it is well known that both the liquefaction resistance and the quasi-elastic stiffness during liquefaction are influenced by aging of the sample (Koseki et al., 1999 and 2001, among others). The change of liquefaction resistance due to sample disturbance, including the loss of aging effect, which is caused by sampling, sample preparation and freeze-thaw process, has been also investigated (Tokimatsu et al., 1986; Goto, 1993; Yoshimi et al., 1994; Teachavorasinskun et al., 1994).

In the present study, static and dynamic small strain characteristics of two different in-situ frozen specimens (FSs) and those of reconstituted specimens (RSs) before and during liquefaction were measured. In addition, the effect of confining pressure during thaw process of the FS on the liquefaction properties was discussed. Finally, attempts were made to evaluate the reduction of liquefaction resistance caused by the sample disturbance based on the change in the small strain stiffness before liquefaction.

[1] Research Associate
[2] Professor

TEST PROCEDURE

Test apparatus and strain measurements

An automated triaxial apparatus illustrated in Fig. 1 was used for this study. The cylindrical specimen was 50 mm in diameter and 100 mm in height. The deviator load was measured with a load cell fixed between the loading piston and the specimen top cap in the cell. The volume change of the saturated specimen was obtained from the amount of pore water expelled from or sucked into the specimen by measuring the water height in a burette that was connected to the specimen with a low-capacity differential pressure transducer. The axial strain of the specimen was measured with two types of transducers; a normal external transducer for large strain, and a pair of LDTs (Goto et al., 1991) for small strain. The static Young's modulus, E_s, was evaluated from the small cyclic stress-strain relationships obtained by LDTs with double amplitude axial strain of approximately 0.002 %.

Since the static Young's moduli of saturated specimen obtained under undrained condition are affected by change of excess pore water pressure and inherent and stress-induced anisotropies, the values of E_s during liquefaction were converted to those under drained condition (denoted as E_v) by using Eqs. (1) and (2) (Tatsuoka et al., 1997). In addition, the static shear moduli, G_s, was calculated from the E_v by using Eq. (3) while considering inherent and stress-induced anisotropies (Tatsuoka et al., 1999).

$$E_v = E_{vu}\frac{1+2(aR^n)^{0.5}\nu_0 x}{1+x} \tag{1}$$

$$x=\frac{1-2(aR^n)^{0.5}\nu_0}{2aR^n\left[1-\nu_0-(aR^n)^{-0.5}\nu_0+2(bE_h/\sigma_h' d)\right]} \tag{2}$$

$$G_s=\frac{E_v}{2(1+\nu_0)}\cdot\frac{2(1-\nu_0)}{1+a\cdot R^n-2\sqrt{a}\cdot R^{n/2}\cdot\nu_0} \tag{3}$$

where R is principle stress ratio (= σ_v'/σ_h'), E_{vu} is vertical Young's moduli under undrained condition, E_h is horizontal Young's moduli under drained condition that are formulated as a function of the current effective horizontal stress σ_h', and d is the diameter of the specimen in cm. Note that the values of the reference Poisson's ratio, ν_0, the parameter regarding the inherent anisotropy of Young's moduli, a, and the parameter regarding the effects of membrane penetration, b, were set to 0.17, 0.8 and 1.7×10^{-3}/ln10, respectively. The power number that is related with the stress-state dependency of Young's moduli, n, was set for every specimen as shown later (Table 1 and 2).

Two sets of accelerometers were used to measure the arrival of P and S waves at two different heights on the side surface of specimen (Fig. 2). P and S waves were generated by two pairs of wave sources (triggers) attached on the top cap, which were excited simultaneously in the vertical and torsional direction, respectively. The Young's and shear moduli by dynamic measurement were evaluated employing equations shown in Fig. 2. To evaluate the travel time, t, of the P and S waves between the two accelerometers, the rise to rise time lag of the measured waves was taken as shown in Fig. 3.

In order to confirm the effect of saturation of specimen on dynamic Young's moduli, E_d, experiments were performed with dry and saturated specimens of Toyoura sand (D_{50}= 0.204 mm, FC= 0.1 %, U_c= 1.6). Figure 4 shows the E_d values of dry and saturated specimens during isotropic consolidation from 30 to 200 kPa. The E_d values of saturated specimen are larger than those of dry specimen consistently in spite of almost the same void ratio as shown in Fig. 4. The possible reason may be the effect of pore water in case of the saturated specimen, because the P wave velocity, V_p, of the pore water is much larger than that of soil skeleton. In this study, therefore, the E_d values of saturated specimen obtained from V_p were not considered as an intrinsic parameter of the soil material, while only dynamic shear moduli, G_d, obtained from the S wave velocity, V_s, was used.

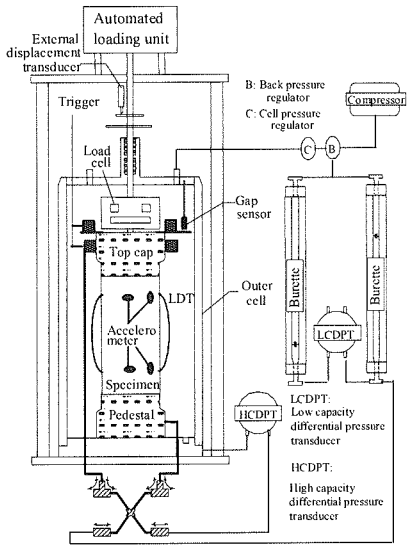

Figure 1. Test apparatus

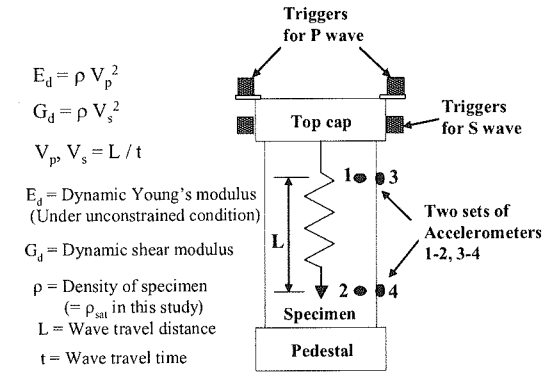

Figure 2. Diagram of P & S wave triggers and accelerometers on a specimen

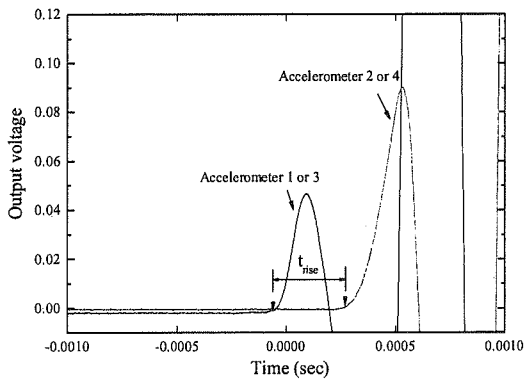

Figure 3. Definition of wave travel time

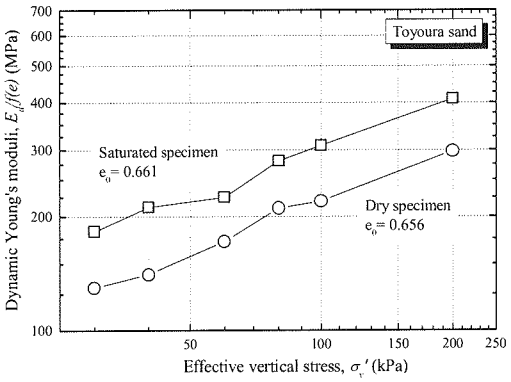

Figure 4. Comparison of E_d between dry and saturated specimen

Specimen preparation and test program

The materials of FS tested in this study were Tone-river Holocene sand (D_{50}= 0.188 mm, FC= 1.2 %, U_c= 2.0) and Edo river Pleistocene sand (D_{50}= 0.189 mm, FC= 2.9 %, U_c= 2.1). The cylindrical specimens with a diameter of 5 cm were cored out of the frozen core samples having a diameter of 15 cm by core cutter machine at a temperature of -20 degrees in the freezer. They were thawed at different confining pressures of 30 kPa and 98 kPa under atmospheric temperature of about 25 degrees, and saturated under the same confining stress, respectively. The volume change of the specimen during the thaw process was manually obtained by measuring the change of the diameter and height of specimen before and after thawing. The RS by using the same material as the FS was prepared by air pluviation of oven-dried particles, and saturated at a confining stress of 30 kPa.

After saturation, the specimens were subjected to isotropic consolidation at a specified confining stress (Tone-river sand: 100 kPa, Edo-river sand: 160 kPa) which is equivalent to the in-situ overburden stress at the depth of sampling, and then undrained cyclic loading was performed. The small strain moduli by static

and dynamic measurements were measured during all these procedures.

After isotropic consolidation, some of the RSs were subjected to 10,000 or 20,000 cycles of axial load with double amplitude axial strain of approximately 0.1 % under drained conditions. This is one of the procedures to increase the liquefaction strength without significantly changing the specimen density (Singh et al, 1982).

TEST RESULTS

Volume change during thaw process

Two series of FSs were thawed at different confining pressures of 30 kPa and 98 kPa, respectively. Figure 5 shows the relationship between the volumetric strain and confining pressure during thaw process of Tone-river sand and Edo-river sand. Larger volumetric strain was observed at higher confining pressure during the thaw process. However, the differences in residual volumetric strain after isotropic consolidation (IC) to 100 kPa (Tone-river sand) and 160 kPa (Edo-river sand) were small as shown in Fig. 5.

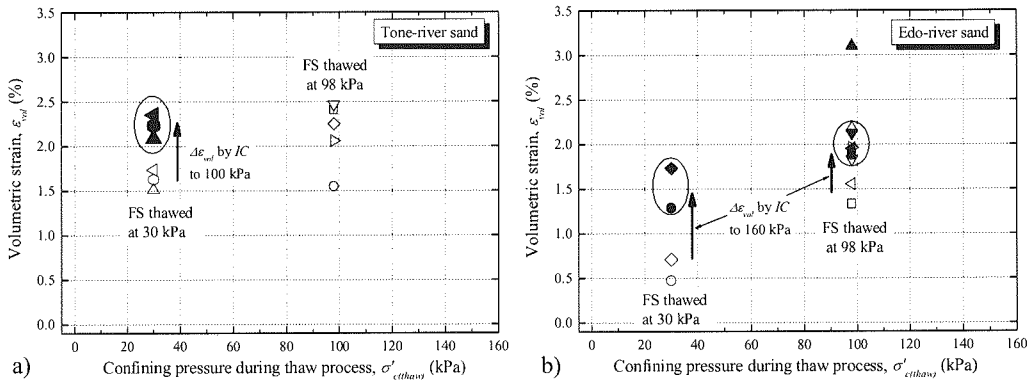

Figure 5. Volumetric strain during thaw process of a) Tone-river sand and b) Edo-river sand

Isotropic consolidation

In this study, in order to correct for the effects of different void ratios, the following function proposed by Hardin and Richart (1963) is applied to normalize the static Young's and shear moduli, E_s and G_s, and dynamic shear moduli, G_d.

$$f(e) = (2.17 - e)^2 / (1 + e) \tag{4}$$

Table 1 shows the values of E_s, n, G_s and G_d of Tone-river sand after isotropic consolidation at 100 kPa. The G_d values were on average 10 to 20 % larger than the G_s. The values evaluated by the dynamic measurement reflect the response of stiff part of the specimen because the wave propagates through the shortest path made by inter-locking of bigger particles. On the other hand, values by static measurement are obtained from global response of the specimen, resulting into smaller stiffness moduli as compared to those by the dynamic measurement.

Figure 6 shows E_s and G_d of Tone-river sand measured during isotropic consolidation from 30 kPa to 100 kPa. Data with thin lines represent the test results of individual specimens. Meanwhile, data with circle symbol, thick line and broken line represent the average value of test results of FS thawed at 98 kPa, the average value of test results of FS thawed at 30 kPa, and the average value of test results of RS, respectively.

Larger small strain stiffness was observed at larger stress level. The average value of E_s of FSs was almost the same as that of RSs. On the other hand, the average value of G_d of FSs was larger than that of

RSs even though both of the specimens had similar void ratios. The values of E_s and G_d of FSs which had been thawed at 98 kPa were larger than those thawed at 30 kPa, and the difference in the G_d values was larger than that in the E_s values. These features suggest that the small strain characteristics, especially G_d, can be employed to identify the sample disturbance caused by low confining pressure during thaw process.

Table 2 shows the values of E_s, n, G_s and G_d of Edo-river sand after isotropic consolidation at 160 kPa. The G_d values were on average 30 to 50 % larger than the values of G_s. Figure 7 shows E_s and G_d of Edo-river sand measured during isotropic consolidation from 30 kPa to 160 kPa. Data with thin lines represent the test results of individual specimens. Meanwhile, data with circle symbols, thick line and broken line represent the average value of test results of FSs thawed at 98 kPa, the average value of test results of FSs thawed at 30 kPa, and the average value of test results of RSs, respectively.

It can be seen that the values of E_s and G_d of FSs were larger than those of RSs. Although the E_s values of the FSs thawed at low pressure were slightly larger than those of FSs thawed at high pressure, the differences between them were relatively small.

The remarkable feature during isotropic consolidation of Tone-river and Edo-river sands was the difference in the E_s and G_d values between FSs and RSs. The E_s and G_d values of FSs were larger than those of RSs in case of Edo-river sand, and the difference was small in case of Tone-river sand. In addition, the small strain stiffness of FSs which were thawed at higher confining pressure was larger than those thawed at lower confining pressure in case of Tone-river sand, and the difference was small in case of Edo-river sand. These features may be explained by the difference in the aging effect that specimens originally had. Although forces between soil particles of FSs may be kept under the in-situ condition by the frozen pore water, they change suddenly when the pore water around the soil particles is thawed. Therefore, thawing at a confining pressure lower than in-situ stress condition makes FSs release suddenly the confining pressure. The FSs of Tone-river sand may be disturbed easily by the low confining pressure during the thaw process because they are Holocene soil, while Edo-river sand Pleistocene sand may have larger resistance against disturbance caused by the low confining pressure.

Because the G_d values were almost similar to the results of in-situ PS logging tests which are shown in Figs. 6 b) and 7 b), it may be inferred that the disturbance of FSs thawed at 98 kPa was very small.

Table 1. Small strain characteristics of Tone-river sand after isotropic consolidation at 100 kPa

	Sample No.	$\sigma'_{c(thaw)}$ (kPa)	Void ratio at 100 kPa	$E_s/f(e)$ (MPa)	n	$G_s/f(e)$ (MPa)	$G_d/f(e)$ (MPa)
FS	TxTon-F1	98	0.720	152.7	-	72.4	89.0
	TxTon-F2	98	0.750	-	-	-	98.6
	TxTon-F3	30	0.715	133.7	0.519	63.4	80.2
	TxTon-F4	98	0.734	148.5	-	70.4	94.8
	TxTon-F5	98	0.764	157.8	-	74.8	99.5
	TxTon-F6	30	0.708	147.3	0.656	69.9	81.2
	TxTon-F7	98	0.725	138.5	-	65.7	83.7
	TxTon-F8	30	0.729	137.3	0.557	65.1	79.7
RS	TxTon-R1	-	0.720	131.6	0.444	62.4	69.1
	TxTon-R2	-	0.763	143.3	0.581	67.9	76.2
	TxTon-R3	-	0.732	115.0	0.622	54.6	76.3
	TxTon-R5	-	0.709	115.3	0.564	54.7	69.8
	TxTon-R6	-	0.692	119.6	0.557	56.7	70.8
	TxTon-R7	-	0.710	110.4	-	52.4	70.8
	TxTon-R8	-	0.730	140.6	0.546	66.7	71.4
	TxTon-R9	-	0.764	141.5	0.558	67.1	77.2
	TxTon-R10	-	0.771	150.9	0.622	71.6	73.1
	TxTon-R11	-	0.764	147.8	0.581	70.1	75.3
	TxTon-R12	-	0.748	135.1	0.547	64.1	62.7
	TxTon-R13	-	0.694	-	-	-	55.8

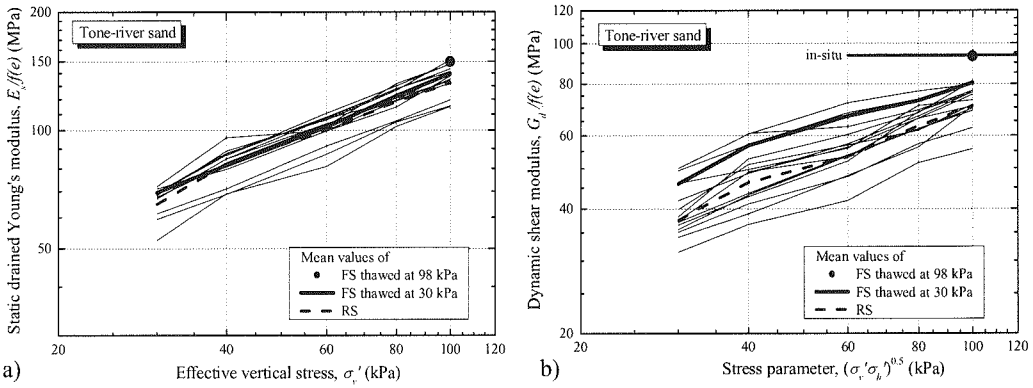

Figure 6. Relationships between a) $E_s/f(e)$-σ'_v, b) $G_d/f(e)$-$(\sigma'_v\ \sigma'_h)^{0.5}$ of Tone-river sand during isotropic consolidation

Table 2. Small strain characteristics of Edo-river sand after isotropic consolidation at 160 kPa

	Sample No.	$\sigma'_{c(thaw)}$ (kPa)	Void ratio at 160 kPa	$E_s/f(e)$ (MPa)	n	$G_s/f(e)$ (MPa)	$G_d/f(e)$ (MPa)
FS	TxEdo-C-F2	30	0.710	333.7	0.589	158.2	244.9
	TxEdo-C-F3	98	0.696	333.4	0.715	158.1	257.6
	TxEdo-C-F4	98	0.818	331.0	0.633	157.0	309.7
	TxEdo-C-F5	30	0.834	388.7	0.604	184.3	295.5
	TxEdo-C-F6	98	0.773	331.1	0.825	157.0	-
RS	TxEdo-C-R1	-	0.755	200.1	0.650	94.9	143.1
	TxEdo-C-R2	-	0.746	203.3	0.675	96.4	146.5
	TxEdo-C-R3	-	0.764	197.8	0.631	93.8	152.5
	TxEdo-C-R4	-	0.780	204.9	0.565	97.2	153.9
	TxEdo-C-R6	-	0.696	209.0	0.537	99.1	140.8
	TxEdo-C-R7	-	0.715	205.9	0.609	97.6	107.1

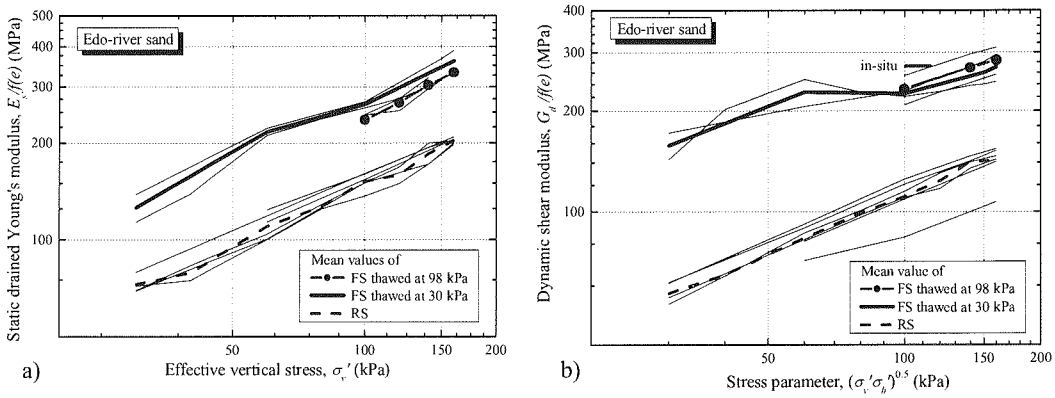

Figure 7. Relationships between a) $E_s/f(e)$-σ'_v, b) $G_d/f(e)$-$(\sigma'_v\ \sigma'_h)^{0.5}$ of Edo-river sand during isotropic consolidation

Effect of shear stress history on small strain characteristics

Some of the RSs were subjected to 10,000 or 20,000 cycles of axial loading with constant double amplitude axial strain, $\varepsilon_{v(DA)}$ of 0.1 % under drained condition after isotropic consolidation. Figure 8 shows the relationship between number of cycles and the small strain characteristics. Increase in the values of E_s and G_d was observed with increase in the number of cycles. The G_d value of the RS with stress history became similar to or larger than the result of in-situ *PS* logging test in case of Tone-river sand. However the G_d value of RS of Edo-river sand could not reach the result of in-situ *PS* logging test even though the number of cycles exceeded 20,000 cycles.

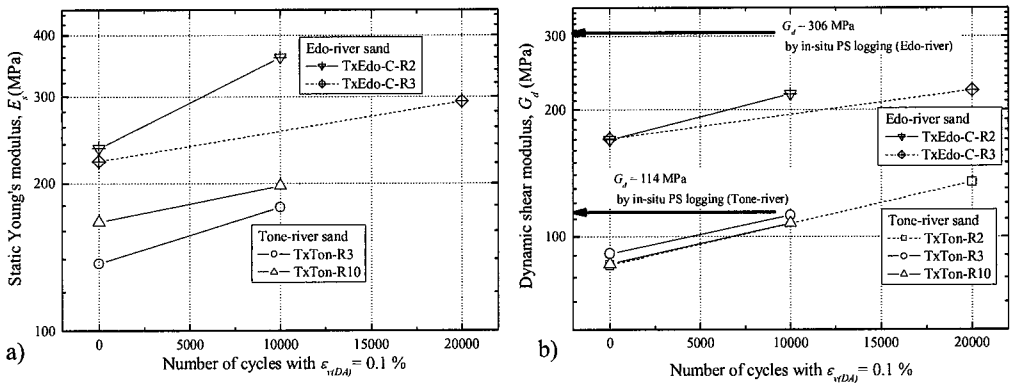

Figure 8. Relationships between number of drained cycles and a) E_s, b) G_d

Liquefaction test

Figure 9 shows the liquefaction test results on a FS of Tone-river sand (TxTon-F6) which was thawed at 30 kPa. As indicated on the stress-path shown in Fig. 9 a), the dynamic shear moduli, G_d, were measured at several stress states, followed by measurement of the static Young's moduli, E_s. Since the values of E_s obtained during liquefaction under undrained condition cannot be compared directly with those during isotropic consolidation that were measured under drained condition, the values of E_s during liquefaction were converted to those under drained condition by using Eqs. (1) and (2).

Figure 9 b) shows the values of E_s of TxTon-F6, which were measured under the isotropic state, triaxial compression (TC) state and triaxial extension (TE) state, plotted versus the effective vertical stress, σ_v'. Decrease in the values of E_s was observed with the decrease in σ_v' during liquefaction. Figure 9 c) shows the values of G_d of TxTon-F6, which were measured under the isotropic state, TC and TE condition, plotted versus an effective stress parameter $(\sigma_v'*\sigma_h')^{0.5}$. The values of G_d during liquefaction decreased with the reduction of the effective stress level. The values of E_s and G_d during liquefaction were equal to or smaller than those during isotropic consolidation under the same stress level. This may suggest that soil structure was less stable during liquefaction than that during isotropic consolidation.

Figure 10 shows the liquefaction test results of a FS of Tone-river sand (TxTon-F4), which was thawed at 98 kPa, which was almost equivalent to the in-situ overburden stress at the sampled depth. While the effective stress path in Fig. 10 a) shows higher liquefaction resistance than that of the specimen thawed at 30 kPa shown in Fig. 9 a), the reduction of small strain characteristics caused by liquefaction in Figs. 10 b) and c) were similar to those shown in Figs. 9 b) and c). In addition, more unique relationships between G_d values and $(\sigma_v'*\sigma_h')^{0.5}$ could be observed as compared with E_s and σ_v' relations.

Figure 11 a) shows the effective stress path and G_d- $(\sigma_v'*\sigma_h')^{0.5}$ relations during the liquefaction process of RS of Tone-river sand (TxTon-R1). Although the void ratio of the RS was almost the same as that of the FS as shown in Table 1, the former required less number of loading cycles to liquefaction. For example, the number of loading cycles to induce double amplitude axial strain, $\varepsilon_{v(DA)}$, of 3 % was 4 and 18 with the RS

(TxTon-R1) and FS (TxTon-F6), respectively. On the other hand, the RS with 20,000 cycles of stress history (TxTon-R3) showed much larger liquefaction resistance as shown in Fig. 12 a). This feature may suggest that strong inter-rocking of soil particles was achieved due to pre-straining by the drained cyclic loading before liquefaction test.

Figures 13 and 14 show the effective stress path and G_d- $(\sigma_v'*\sigma_h')^{0.5}$ relations during liquefaction test of the FS of Edo-river sand (TxEdo-C-F2) and the RS with 20,000 cycles of stress history (TxEdo-C-R3). Although the G_d value before liquefaction test of TxEdo-C-R3 increased due to the stress history as shown in Fig 8 b), the number of loading cycles to induce double amplitude axial strain, $\varepsilon_{v(DA)}$, of 3 % was 6 with the RS (TxEdo-C-R3), which was smaller than 12 as obtained with the FS (TxEdo-C-F2).

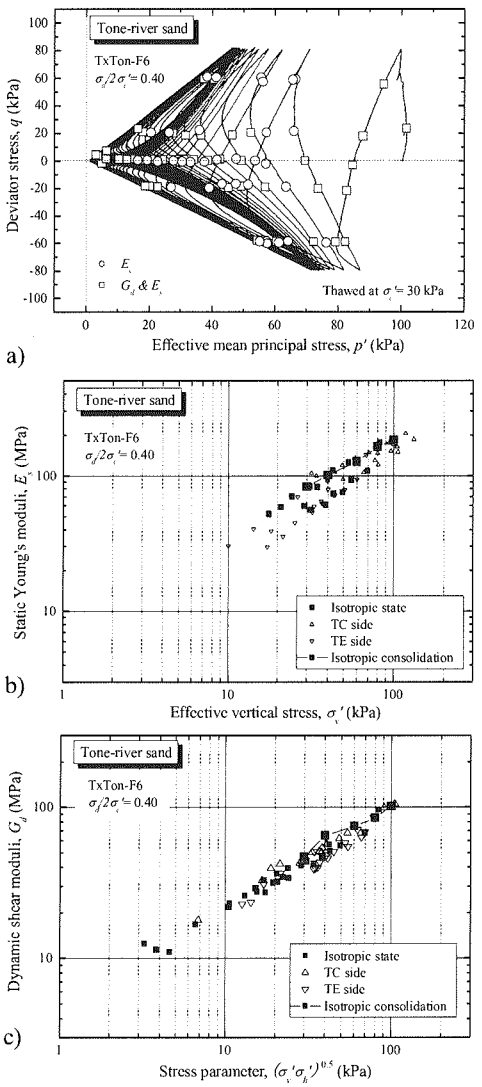

Figure 9. a) Stress path, b) E_s and c) G_d, during liquefaction test on FS of Tone-river sand thawed at 30 kPa

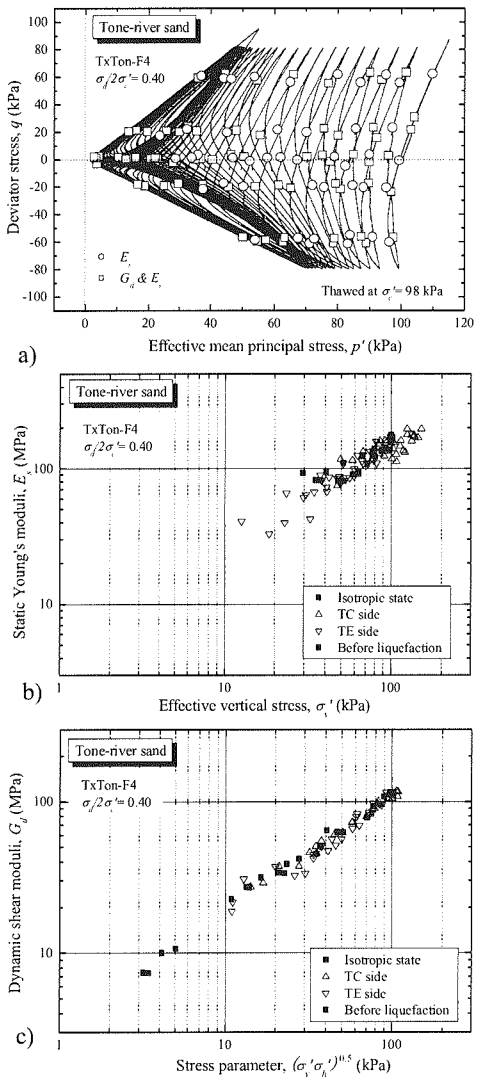

Figure 10. a) Stress path, b) E_s and c) G_d, during liquefaction test on FS of Tone-river sand thawed at 98 kPa

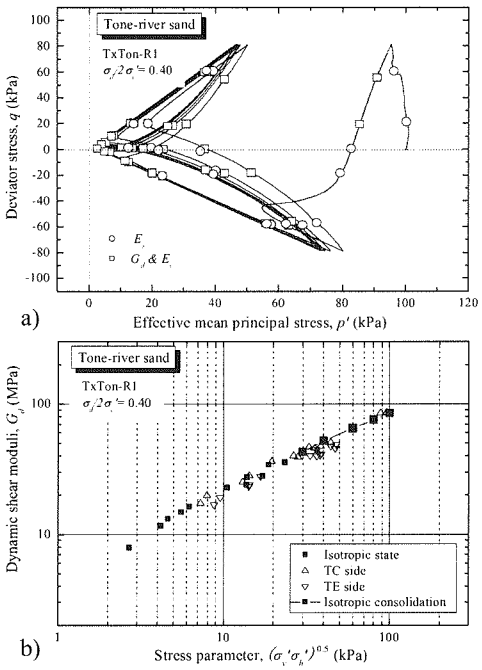

Figure 11. a) Stress path and b)G_d, during liquefaction test on RS of Tone-river sand

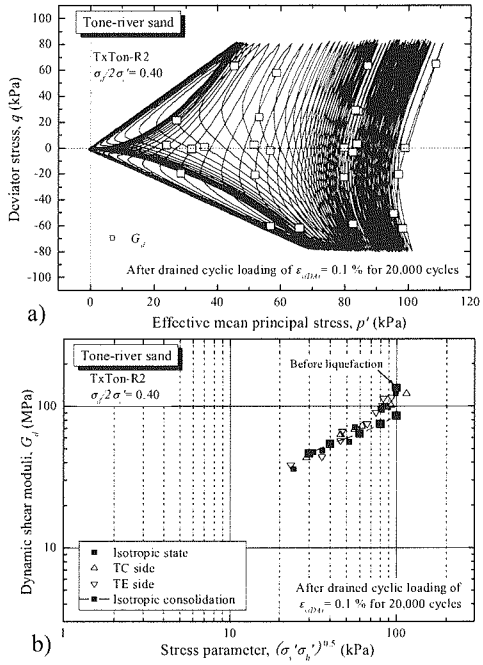

Figure 12. a) Stress path and b)G_d, during liquefaction test on RS of Tone-river sand with stress history of 20,000 cycles

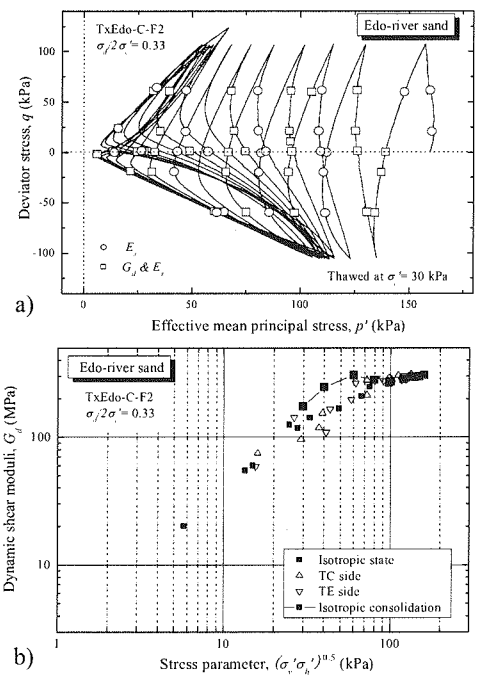

Figure 13. a) Stress path and b) G_d, during liquefaction test on FS of Edo-river sand thawed at 30 kPa

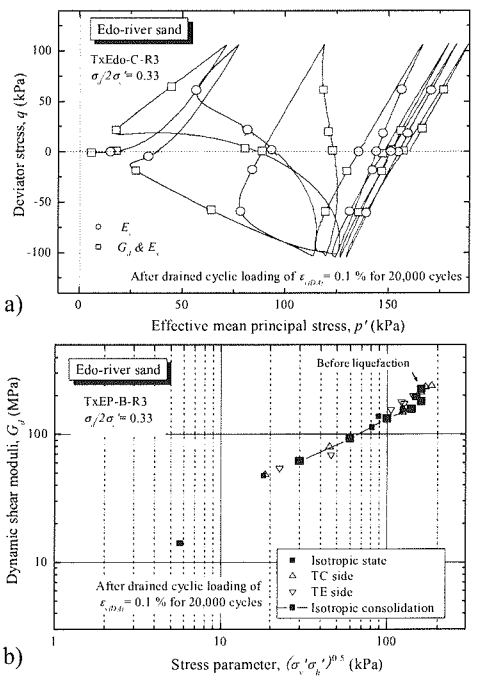

Figure 14. a) Stress path and b) G_d, during liquefaction test on RS of Edo-river sand with stress history of 20,000 cycles

Figure 15 compares the reduction of G_d values caused by liquefaction between the FS and the RS with a number of cyclic loading (CL) histories. Note that the value of G_d was normalized by G_0 that was measured immediately before the liquefaction test in Fig. 15. In the case of the FS and the RS of Tone-river sand and the RS of Edo-river sand, a sudden reduction of G_d/G_0 was observed at an initial part of the liquefaction process. On the other hand, a slower reduction of G_d/G_0 was observed at an initial part of liquefaction in the case of FS of Edo-river sand. This feature may imply that the particle fabric of the RSs, which is structured by cyclic loading history, disappears easily. On the other hand, in case of the FSs, since Edo-river sand is Pleistocene soil, the G_d/G_0 value does not decrease easily due to its natural aging effect. However, since Tone-river sand is Holocene soil, even the FS may not have such natural aging effect.

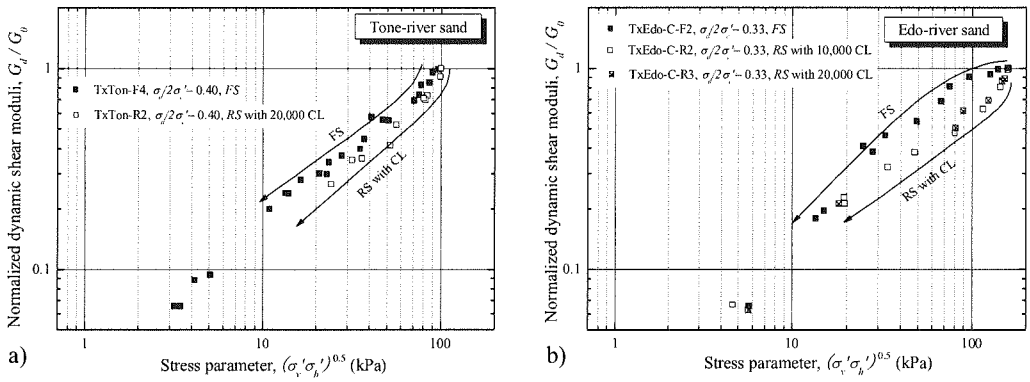

Figure 15. Comparison of normalized dynamic shear moduli, G_d/G_0 between frozen and reconstituted specimens on a) Tone-river sand and b) Edo-river sand

DISCUSSION

While the differences in the residual volumetric strains of FSs at different confining pressures during thaw process were relatively small, the values of quasi-elastic modulus, E_s and G_d, after isotropic consolidation were affected by the difference in the confining pressures during the thaw process, especially in case of Tone-river sand. In addition, increase in E_s and G_d values was observed after applying a number of cyclic loading (CL) histories. Therefore, the liquefaction resistances of FSs and RSs, which undergo different stress histories, may be linked to each other.

Figure 16 shows the relationships between shear stress ratio and number of cycles required to cause $\varepsilon_{v(DA)}$= 3 % for both a) Tone-river and b) Edo-river sands. The liquefaction resistance of RSs was much smaller than that of FSs even if the void ratio is similar to each other as shown in Tables 1 and 2. However, increase in the liquefaction resistance was observed after applying drained cyclic shearing on RSs, and the liquefaction resistance seems to be linked with the number of drained cyclic loading before liquefaction test. In addition, the influence of the confining pressure during thaw process of Tone-river FSs on the liquefaction resistance was larger than that of Edo-river FSs.

Figures 17 and 18 show the relationships between liquefaction resistance R_{L15}, defined as the shear stress ratio to cause $\varepsilon_{v(DA)}$= 3 % at 15 cycles, and the static Young's modulus, E_0, and the dynamic shear modulus, G_0, which were measured immediately before starting liquefaction tests. As shown in Figs. 17 b) and 18 b), the relationships between G_0 and R_{L15} were more unique than those between E_0 and R_{L15} as shown in Figs. 17 a) and 18 a). Especially, the R_{L15} and G_0 values of the RSs of Tone-river sand with shear history of 10,000 cycles corresponded to those of the FSs thawed at 98 kPa. These trends suggest that dynamic shear moduli measured before liquefaction test may reflect the liquefaction resistance of both RSs and FSs

including the effect of specimen disturbance due to different confining pressures during thaw process. In other words, RSs with a value of G_0 that is similar to the in-situ *PS* logging test result may be used to estimate liquefaction behaviour instead of using FSs. However, the trends of reduction in the G_d values during liquefaction test on Edo-river sand were different between FS and RSs as shown Fig 15 b). Therefore, it seems that there is a limitation in reproducing the liquefaction behaviour by using RSs even if small strain characteristics are adjusted to those of FSs.

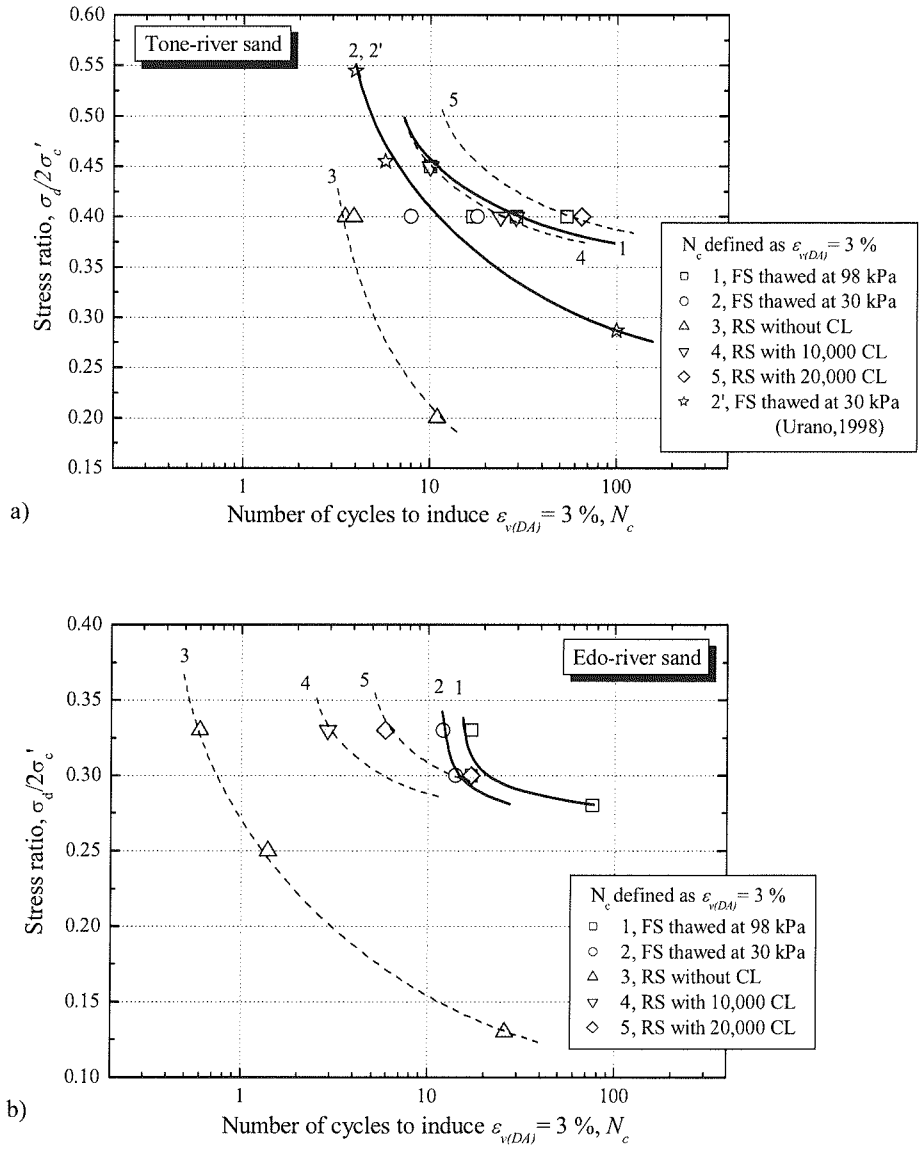

Figure 16. Liquefaction characteristics of FS and RS of a) Tone-river sand and b) Edo-river sand

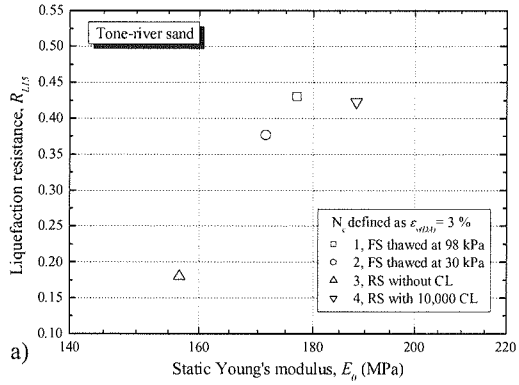

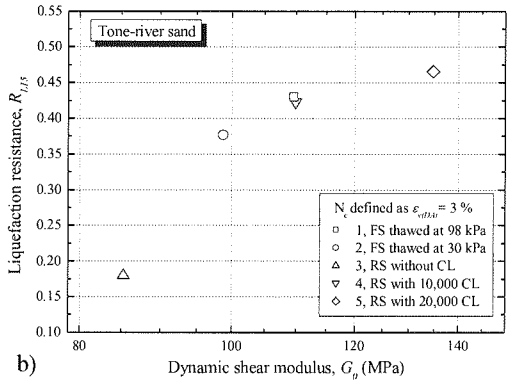

Figure 17. Relationships between liquefaction resistance and a) E_0 and b) G_0 of Tone-river sand

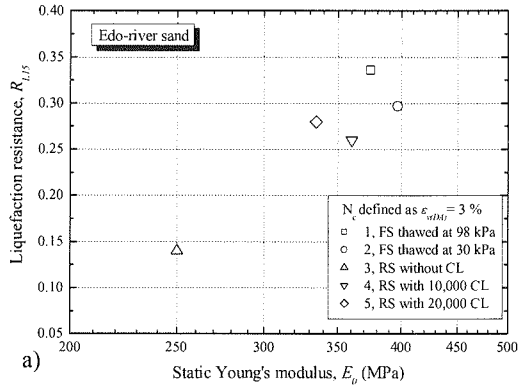

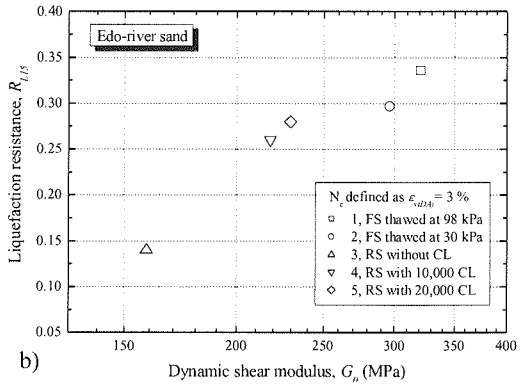

Figure 18. Relationships between liquefaction resistance and a) E_0 and b) G_0 of Edo-river sand

CONCLUSIONS

The present paper includes comparison of liquefaction properties of in-situ frozen specimens (FSs) and reconstituted specimens (RSs) and their small strain characteristics. The following conclusions can be drawn from test results.

1) The volumetric strain of FSs was affected by the level of confining pressure during thaw process, while the difference in the residual volumetric strains at the end of isotropic consolidation was insignificant.
2) Decrease in small strain stiffness was observed in FSs of Tone-river Holocene sand that was thawed at lower confining pressure.
3) Large difference in the small strain stiffness between FSs and RSs was observed during isotropic consolidation stage of Edo-river Pleistocene sand, while the difference with Tone river Holocene sand was small.
4) The values of small strain stiffness, especially dynamic shear moduli evaluated by S-wave measurement, G_d, may be used to identify the loss of the aging effect of the specimen. It may be also useful in estimating the liquefaction resistance, which is affected by the difference in the conditions of sample preparation including thaw process.
5) In the case of FSs and RSs of Tone-river sand and RSs of Edo-river sand, a sudden reduction of G_d was observed at an initial part of the liquefaction process. On the other hand, a slower reduction of G_d was

observed at an initial part of liquefaction in the case of FSs of Edo-river sand. This feature may suggest that there is a limitation in reproducing liquefaction behaviour of natural aged soil deposit by using RSs even if small strain characteristics are adjusted to those of FSs.

REFERENCES

Urano, I. (1998): Liquefaction properties of in-situ frozen sandy sample in undrained triaxial cyclic loading tests, Bachelor of Eng. Thesis, Nihon Univ. (in Japanese)

Goto, S., Tatsuoka, F., Shibuya, S., Kim, Y.S. and Sato, T. (1991): A simple gauge for local small strain measurement in the laboratory, *Soils and Foundations*, **31** (1), 169-180.

Goto, S. (1993): Influence of a freeze and thaw cycle on liquefaction resistance of sandy soils, *Soils and Foundations*, **33** (4), 148-158.

Hardin, B.O. and Richart, F.E. (1963): Elastic wave velocities granular soils, *Journal of ASCE*, **89** (1), 33-65.

Koseki, J., Sato, T., Maeshiro, N. and Urano, I. (1999): Elastic deformation properties of sands containing fines during liquefaction, *Physics and Mechanics of Soil Liquefaction*, Balkema, 121-132.

Koseki, J., Kawakami, S., Nagayama, H. and Sato, T., (2000): Change of small strain quasi-elastic deformation properties during undrained cyclic torsional shear and triaxial tests of Toyoura sand, *Soils and Foundations*, **40** (3), 101-110.

Koseki, J. and Ohta, A. (2001): Effects of different consolidation conditions on liquefaction resistance and small strain quasi-elastic deformation properties of sands containing fines, *Soils and Foundations*, **41** (6), 53-62.

Singh, S., Seed, H.B. and Chan, C.K. (1982): Undisturbed sampling of saturated sand by freezing, *Journal of the Geotechnical Engineering Division*, Proc. of ASCE, Vol.108, GT2, 247-268.

Tanizawa, F., Teachavorasinskun, S., Yamaguch, J., Sueoka, J. and Goto, S. (1994): Measurement of shear wave velocity of sand before liquefaction and during cyclic mobility, *Pre-failure deformation of geomaterials*, Balkema, 63-68.

Tatsuoka, F., Jardine, R.J., Lo Presti, D., Di Benedetto, H. and Kodaka, T. (1997): Characterising the pre-failure deformation properties of geomaterials, *Proc. of 14th ICSMFE*, **4**, 2129-2164.

Tatauoka, F., Ishihara, M., Uchimura, T. and Gomes Correia, A. (1999): Non-linear resilient behaviour of unbound granular materials predicted by the cross-anisotropic hypo-quasi-elasticity model, *Proc. of Workshop on Modelling and Advanced testing for Unbound Granular Material*, Balkema, 197-204.

Teachavorasinskun, S., Tatsuoka, F. and Lo Presti, D.C.F. (1994): Effects of the cyclic prestraining on dilatancy characteristics and liquefaction strength of sand, *Pre-failure Deformation of Geomaterials*, Balkema, **1**, 75-80.

Tokimatsu, K. and Hosaka, Y. (1986): Effects of sample disturbance on dynamic properties of sand, *Soils and Foundations*, **26** (1), 53-64.

Yoshimi, Y., Hatanaka, M. and Ohoka, H. (1978): Undisturbed sampling of saturated sands by freezing, *Soils and Foundations*, **18**(3), 59-73.

Yoshimi, Y., Tokimatsu, K. and Ohara, J. (1994): In situ liquefaction resistance of clean sands over wide density range, *Geotechnique*, **44** (3), 479-494.